



The influence of different simplified sliding-block models and input parameters on regional predictions of seismic landslides triggered by the Northridge earthquake



Daniel Dreyfus^a, Ellen M. Rathje^{a,*}, Randall W. Jibson^b

^a University of Texas at Austin, Department of Civil, Architectural, and Environmental Engineering, 301 E. Dean Keeton St., Stop C1700, Austin, TX 78712, United States

^b U.S. Geological Survey, Denver Federal Center, Box 25046, MS 966, Denver, CO 80225, United States

ARTICLE INFO

Article history:

Received 23 July 2012

Received in revised form 22 May 2013

Accepted 25 May 2013

Available online 10 June 2013

Keywords:

Northridge earthquake

Landslide

Seismic hazards

Seismic slope stability

ABSTRACT

Regional seismic landslide hazard maps are based on predictions of rigid-sliding-block displacement derived from estimates of earthquake ground shaking, topography, geology, and shear strength. The confidence in these predictions requires comparisons with field observations of landslide occurrence during previous well-documented earthquakes. This paper presents a comparison between observed landslides from the 1994 Northridge, California earthquake and predicted landslides based on sliding-block displacement estimates. Seven empirical displacement models, each of which uses a different combination of ground-motion parameters, are investigated to evaluate which models and associated ground-motion parameters best predict seismic landslides. Using best estimates of ground shaking and shear-strength properties from the Northridge earthquake, sliding displacements are calculated and compared with the locations of observed landslides. Only 20–40% of the observed landslides are captured and the total area of predicted landslides is much larger than observed. The ability to predict landslide occurrence accurately depends less on the displacement model and associated ground-motion parameters, and more on the uncertainty in the model parameters, particularly the assigned shear-strengths. Because current approaches do not take into account the spatial variability of shear strength within individual geologic units, the accuracy of the predictive models is controlled predominantly by the distribution of slope angles within a geologic unit. Assigning overly conservative (low) shear-strength values results in a higher percentage of landslides accurately identified but also results in a large over-estimation of the total landslide area. Making more accurate maps of seismic landslide hazards will require methods to define intra-formational variations in shear strength.

© 2013 Elsevier B.V. All rights reserved.

1. Introduction

Regional maps that predict the locations of earthquake-triggered landslides commonly are based on estimates of rigid-sliding-block displacements (Newmark, 1965) because these displacements have been correlated with the occurrence of landslides from previous well-documented earthquakes. Wilson and Keefer (1983) showed that the sliding-block model can accurately predict the co-seismic displacement of an individual landslide, and Jibson et al. (2000) demonstrated that regional estimates of sliding-block displacement correlate strongly with mapped locations of seismically triggered landslides. Although the sliding-block model theoretically applies only to block-type landslides that fail primarily by basal shear, Jibson et al. (2000) and McCrirk (2001) showed that predicted sliding-block displacements also correlate very well with the occurrence of disrupted falls and slides in rock and debris, which are the most abundant types of earthquake-generated landslides (Keefer, 1984) and which occur through a combination of tensile

and shear failure. Since the Jibson et al. (2000) and McCrirk (2001) studies, the use of the sliding-block model to evaluate regional seismic landslide hazards has come into general usage (e.g., Carro et al., 2003; Jibson and Michael, 2009; California Geological Survey, 2013), and methods are under development to use these models for rapid prediction of landslide occurrence after earthquakes using ground-motion estimates from products such as ShakeMap (Godt et al., 2009; U.S. Geological Survey, 2012). Given the widespread usage of the sliding-block model, this paper does not address its appropriateness but rather its utility. The landslide distributions predicted by different predictive models for rigid-block displacement are evaluated and the effects of variation of the key input parameters are quantified.

Applying the sliding-block model to predict earthquake-induced landslides at regional scale involves integration of topographic, geologic, geotechnical, and seismological information to develop estimates of sliding displacement. Topographic, geologic, and geotechnical (shear-strength) data are used to generate maps of yield acceleration (i.e., k_y , the acceleration that results in a factor of safety of 1.0 for the slope), and the yield acceleration is combined with the predicted level of ground shaking to estimate displacement. Generally, the topography and geology can be characterized accurately; therefore, the principal sources of uncertainty

* Corresponding author. Tel.: +1 512 232 3683; fax: +1 512 471 6548.

E-mail addresses: danieldreyfus@gmail.com (D. Dreyfus), e.rathje@mail.utexas.edu (E.M. Rathje), jibson@usgs.gov (R.W. Jibson).

in existing modeling procedures are the characterization of shear strength and seismic ground motion. A further complication is that several different empirical relationships for estimating rigid-sliding displacement have been published (e.g., Jibson, 2007; Saygili and Rathje, 2008), but the differences between results from these models have not been quantified.

This paper addresses two fundamental questions in this maturing field of study: (1) Are there significant differences between the landslide distributions predicted by published models that predict sliding-block displacement, and, if so, which models yield the best results? (2) How sensitive are model results to different shear-strength models? These questions are addressed by comparing the results of the various models and input parameters to the occurrence of landslides triggered by the 1994 $M_w = 6.7$ Northridge, California earthquake (Harp and Jibson, 1995, 1996). The Northridge inventory includes more than 11,000 landslides and is perhaps the best-documented inventory of earthquake-induced landslides yet published. This paper describes the data sets and procedures used in the comparison, presents accuracy assessments for the different empirical models and input parameters considered, interprets the results, and provides recommendations for future research directions that could improve current mapping procedures.

2. Previous seismic landslide comparison studies

The two most important seismic landslide comparison studies analyzed the landslide inventories from the 1994 $M_w 6.7$ Northridge earthquake (Jibson et al., 2000) and the 1989 $M_w 6.9$ Loma Prieta, California earthquake (McCrink, 2001). These studies used similar frameworks in which sliding-block displacements were predicted across the study area within a Geographic Information System (GIS) and compared with the mapped locations of landslides triggered by the earthquake. The basic framework is described below, followed by a description of the results from these studies.

A map of yield acceleration (k_y) is generated assuming an infinite-slope condition (Figure 1). If one considers earthquake shaking to occur parallel to the slope, the yield acceleration can be expressed as a simple function of the static factor of safety (FS), the acceleration of gravity (g), and the slope angle (α):

$$k_y = (FS - 1) \cdot g \cdot \sin(\alpha) \quad (1)$$

Based on the slope geometry (the slope-normal thickness of the rigid sliding block, t ; the proportion of the block thickness that is saturated, m ; and the slope angle, α , Figure 1) and the soil properties (the effective cohesion, c' ; effective friction angle, ϕ' ; and material unit weight, γ) the static factor of safety for an infinite-slope model is computed as:

$$FS = c' / (\gamma \cdot t \cdot \sin \alpha) + \tan \phi' / \tan \alpha \cdot (1 - m \cdot \gamma_w / \gamma) \quad (2)$$

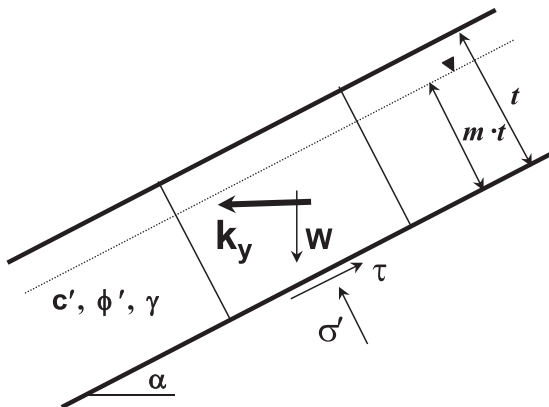


Fig. 1. Infinite slope model for stability calculations.

For regional applications of the infinite-slope model, slope angles are derived from a Digital Elevation Model (DEM), and nominal values for unit weight, block thickness, and saturation thickness are assumed. A 10-m DEM is recommended (Jibson et al., 2000) such that k_y values are developed for a 10-m grid. The main sources of uncertainty in calculating FS and k_y are the assigned material shear strength and thickness of the rigid sliding block. Shear strength is assigned using strength parameters c' and ϕ' obtained from direct shear or triaxial tests. These parameters relate the shear strength to the effective stresses present on the failure plane. Shear-strength data typically are compiled and assigned based on geologic units. Variability within a geologic unit is ignored due to practical constraints. When the shear-strength parameters include non-zero cohesion the sliding-block thickness plays an important role in defining the yield acceleration. k_y increases with decreasing thickness and the effect is significant when the thickness is less than about 2 m. However, the measured shear-strength parameters typically are not representative of the low confining pressures associated with a small sliding-block thickness. Thus, care must be taken to select a sliding-block thickness that is appropriate and consistent with the stress range over which the strength parameters were developed.

The k_y information essentially is a map of seismic landslide susceptibility because it does not predict sliding displacement or landslide occurrence. To develop a map that predicts landslide occurrence, the k_y information is combined with earthquake shaking information to estimate sliding displacement. For regional applications, the ground-shaking level is selected based on a seismic hazard map that defines peak ground accelerations (PGA) or any other ground-motion parameter for a given hazard level, such as 10% probability of exceedance in 50 years (Jibson and Michael, 2009). Having defined the ground shaking and k_y information, displacements are predicted for each 10-m grid cell using an empirical sliding-displacement model or time histories selected to represent the characteristics of shaking. Cells having displacements greater than a specified threshold are predicted to trigger landslides. Commonly used displacement thresholds are 5 and 15 cm (California Geological Survey, 2004; Jibson and Michael, 2009).

2.1. Jibson et al. (2000) study

Jibson et al. (2000) considered six 7.5' quadrangles in the Santa Susana Mountains north of Los Angeles, California that were shaken by the 1994 Northridge earthquake. This was the first earthquake for which a comprehensive data set of slope and soil information, ground shaking, and observed landslides was available to permit a detailed regional analysis. They calculated slope angles from a 10-m DEM and assigned soil shear strengths (c' , ϕ') based on results of direct-shear tests from local geotechnical consultants on samples of geologic units in the region. All data used in the study were imported into a GIS platform and converted to layers of gridded raster data at 10-m cell spacing.

Displacements were predicted using an empirical displacement model developed as part of the study (Jibson et al., 2000). This model estimated displacements as a function of k_y and the Arias shaking intensity (I_a , Arias, 1970). To estimate I_a on a regional 10-m grid spacing, they computed the average I_a for the two horizontal components of recorded ground motion from the Northridge earthquake at 189 strong-motion stations and interpolated across the study area using a simple kriging algorithm. The interpolated values of I_a ranged from less than 1 m/s in the northwest corner of the study area to about 5 m/s in the southeast corner, closest to the fault rupture.

Maps of predicted displacement were compared with locations of mapped landslides from Harp and Jibson (1995, 1996). Visual comparisons within a small zone of the larger study area indicated that areas having large predicted displacements generally corresponded to observed landslide locations. Jibson et al. (2000) also quantitatively evaluated a probability of failure (P_f) for different ranges of displacements. Probability of failure was defined as the percentage of cells within a displacement bin that were occupied by landslide source cells, and this probability was

computed for different levels of predicted displacement (Figure 2a). The results indicated that the probability of landslide occurrence increased monotonically with increasing predicted landslide displacement. However, the probability of failure never exceeded about 34% even at very large displacements, which suggests that no more than 34% of high landslide hazard areas are likely to experience failure during an earthquake.

2.2. McCrink (2001) study

McCrink (2001) used landslides observed from the 1989 Loma Prieta, California earthquake in the Laurel 7.5' quadrangle in the Santa Cruz Mountains to evaluate regional landslide prediction procedures. The landslide inventory was developed from a compilation of maps and reports developed by various geologists. Values of k_y were computed using slope angles from a 10-m DEM and geotechnical shear strengths derived from laboratory testing from different geologic units. In contrast to other studies, McCrink (2001) used a single recorded ground-motion time series to develop the relationship between k_y and sliding displacement. This motion was recorded in the Santa Cruz Mountains during the Loma Prieta earthquake and was considered representative of shaking across the quadrangle.

McCrink (2001) compared the landslide inventory with the locations of predicted landslides for different modeling assumptions and parameters. The parameters c' and ϕ' , the thickness of the failure

mass (t), the saturation thickness (m), and the displacement threshold used to identify landslides all were modified to find the combination of values that accurately predicted the most landslides. Parameter sets were evaluated based on maximizing the percentage of landslide cells accurately identified (%GFC = % Ground Failure Capture) and minimizing the percentage of the quadrangle identified as landslides (%QC = % Quadrangle Covered). This second criterion was implemented by maximizing the difference between %GFC and %QC (%Difference = %GFC – %QC), which penalizes parameter sets that have a large %GFC simply by predicting a large landslide area (%QC).

The results from McCrink (2001) are shown in Fig. 2b in terms of the computed %Difference versus %GFC for a displacement threshold of 5 cm and different parameter sets. This plot was used by McCrink (2001) to select a parameter set that maximized %GFC while maintaining a large %Difference. The selected parameter set labeled “best” in Fig. 2 captured 84% of the landslides (%GFC = 84%) with a %Difference of 34%, which corresponds to 50% of the quadrangle being identified as landslides (i.e. %QC = 50%). The selected best parameter set represents an average friction angle, zero cohesion ($c' = 0$), unsaturated slope conditions ($m = 0$), and a displacement threshold of 5 cm. The current seismic landslide maps developed by the California Geological Survey (CGS) use this parameter set.

3. Description of study

The approach used in this study is similar to that used in previous studies: compare locations of observed earthquake-induced landslides to locations of large predicted displacements. However, the goal of this study was to investigate the influence of the different displacement models and input parameters on the comparison between observed and predicted landslides. The landslides induced by the 1994 Northridge earthquake in the six quadrangles located in the Santa Susana Mountains were selected for study based on the availability of the comprehensive landslide inventory developed by Harp and Jibson (1995, 1996).

3.1. Generation of k_y maps

Data were compiled in a GIS for six 7.5' quadrangles (Piru, Val Verde, Newhall, Simi Valley, Santa Susana, and Oat Mountain) in the Santa Susana Mountains (Figure 3) north of the San Fernando Valley and the main rupture of the Northridge earthquake. Slope angles across the study area were defined at 10-m spacing using the same DEM used by Jibson et al. (2000). The DEM and slope-angle information are shown in Fig. 4 for the Oat Mountain quadrangle. The spatial distribution of geologic units across all six quadrangles is based on 1:24,000-scale geologic maps of Yerkes and Campbell (1995a,b,c,d, 1997a,b), the same maps used by Jibson et al. (2000).

Representative shear strengths were assigned to the geologic units using the shear strengths published by the CGS in their Seismic Hazard Reports for each quadrangle (California Department of Conservation, 1997a,b,c, 2002a,b). The shear-strength data gathered by CGS are primarily from geotechnical reports prepared by consultants and on file with local government permitting departments. Tests generally were from samples taken within a few meters of the ground surface, the zone most likely to produce landslides during earthquakes. In cases where shear-test data were limited, test results from adjacent quadrangles were used to augment the data. The CGS reports group geologic units together into Strength Groups based on their average friction angle, lithologic character, and bedding conditions (adverse vs. favorable), and each Strength Group is assigned a single representative value of ϕ' for use in stability analyses. Although CGS did not use cohesion in their stability analyses, they did publish values of c' in their reports. Using the shear strengths and geologic descriptions provided in the CGS reports, median values of c' and ϕ' were assigned to all geologic units. Table 1 lists the values of c' and ϕ' assigned to each geologic unit within each quadrangle; values of c' range from 12 to 35 kPa, and values of ϕ' range from 12° (for pre-existing landslide

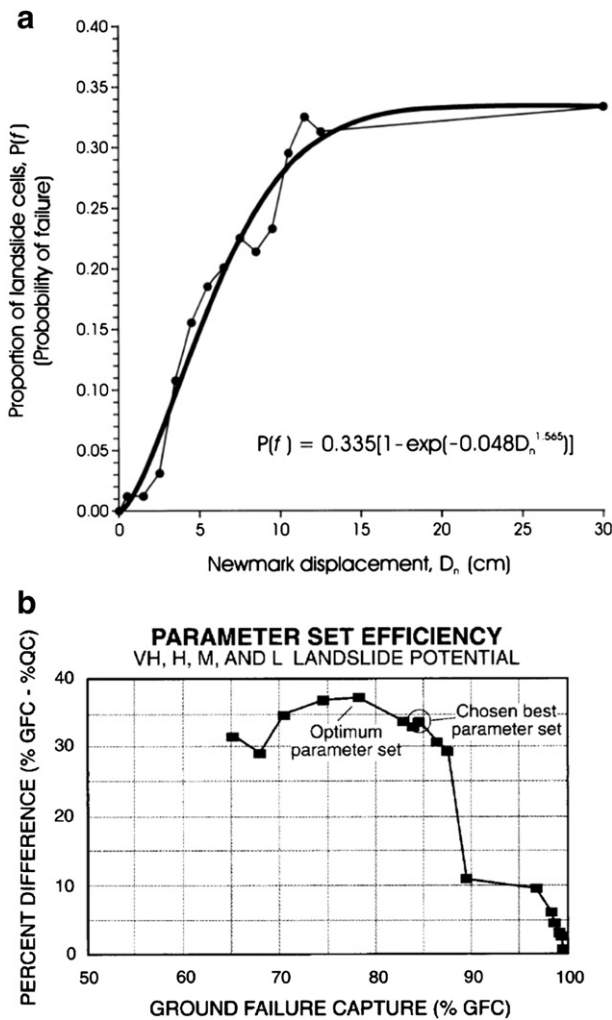


Fig. 2. Results from previous regional seismic landslide studies. (a) Probability of seismic landslide occurrence for different predicted sliding displacement levels from Jibson et al. (2000). (b). Identification of chosen best parameter set for the prediction of earthquake-induced landslides from McCrink (2001).

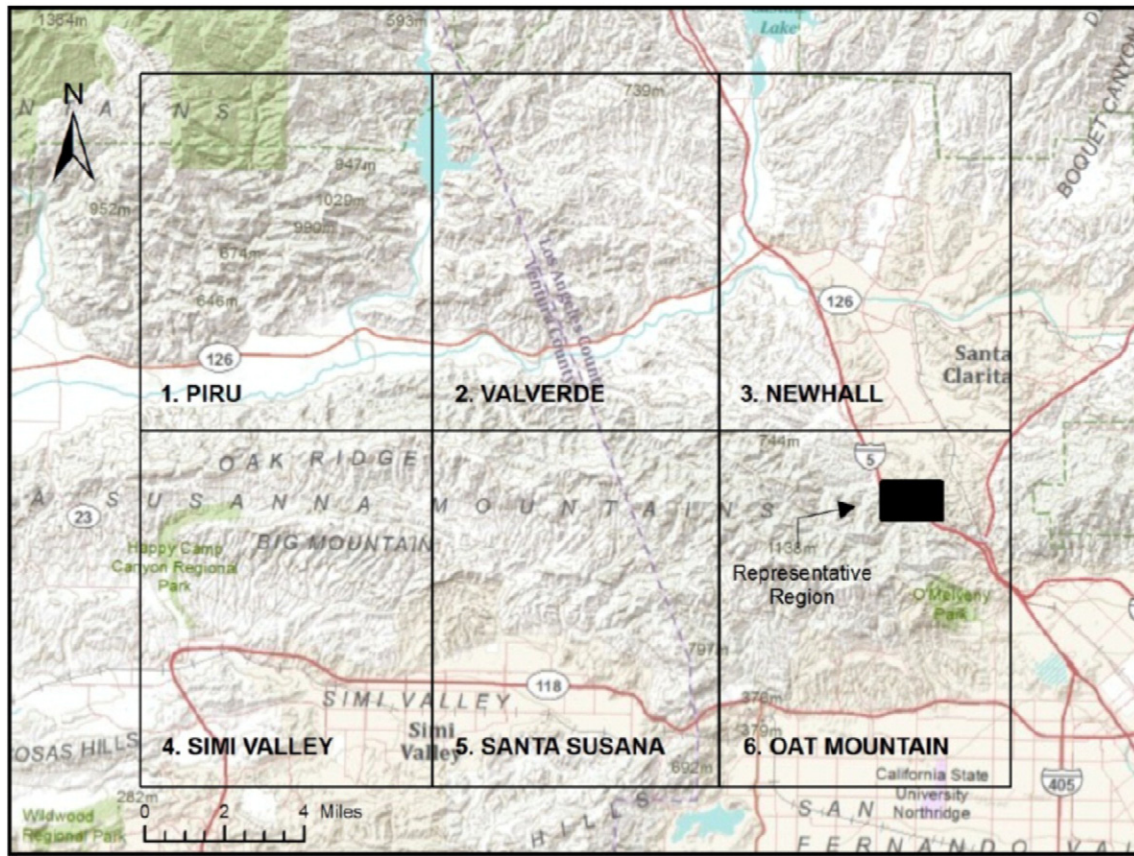


Fig. 3. Locations of quadrangles investigated in this study.

deposits, QIs) to 39° (for well-cemented Cretaceous and Tertiary units). The mapped locations of the four Strength Groups in the Northridge earthquake quadrangle are shown in Fig. 4(c).

In calculating k_y from the strength information using Eqs. (1) and (2), the following assumptions are made. The contribution of pore-water pressure to the effective stress on the failure plane is considered negligible ($m = 0$) because landslides in the Northridge earthquake occurred in dry conditions (Jibson et al., 2000). To be consistent with the previous work by Jibson et al. (2000), a unit weight (γ) of 15.7 kN/m^3 and a sliding-mass thickness (t) of 2.4 m are used to represent a typical slope failure from the Northridge earthquake. The effect of the assigned thickness is not investigated in this research because it was well-characterized during reconnaissance of the Northridge earthquake. However, it does represent a source of uncertainty that influences the results. The resulting k_y map for the Oat Mountain quadrangle is shown in Fig. 4(d). The most susceptible slopes having the smallest k_y are concentrated in Strength Groups 2 and 3 within the northern part of the quadrangle, where slopes are steepest. Maps for the other quadrangles are in Dreyfus (2011).

Shear strengths listed in Table 1 generally are lower than those used by Jibson et al. (2000) for the same quadrangles. Jibson et al. (2000) began the analysis by using median strengths compiled from direct-shear tests provided by local geotechnical consultants; these values were increased until all slopes less than 60° had a static factor of safety greater than 1.0. Jibson et al. (2000) stated that keeping intact the relative strength differences between geologic units was more important than the absolute values. However, this approach overestimates the strength of an entire geologic unit if that unit contains some very steep slopes. The steepest areas within a geologic unit are likely to have the highest local strengths within that unit; thus, using the steepest slopes to calibrate the strength of an entire unit results in overestimating the strength of the flatter slopes within that unit. Therefore, in this study

the median shear strengths are used throughout a geologic unit even if those strengths result in the steepest slopes in that unit being statically unstable. These steeper slopes were then assigned a static FS of 1.01. This artificial approach to handling very steep slopes is needed because of the current inability to map spatial variations in strengths within geologic units.

The influence of the assigned shear strengths on the distribution of k_y is significant. Fig. 5 shows a histogram of k_y values across the Oat Mountain quadrangle computed from the strengths used by Jibson et al. (2000), the strengths used in this study (Table 1), and strengths assigned from the friction angles in Table 1 with $c' = 0$ (CGS approach). The high shear strengths used by Jibson et al. (2000) result in very few (<1%) k_y values below 0.3 g, which implies that the landslide susceptibility across the entire quadrangle is low. The McCrink (2001) approach, which ignores the contribution of cohesion to the shear strength, results in about 15% of the quadrangle being statically unstable ($FS \leq 1$, $k_y = 0.0 \text{ g}$) and nearly 50% of the quadrangle having a yield acceleration less than 0.3 g. The strengths used in this study result in a small percentage of the quadrangle being statically unstable (0.4%) and about 10% of the quadrangles having a yield acceleration less than 0.3 g.

3.2. Estimates of ground shaking

Ground shaking from the Northridge earthquake was characterized across the region using ShakeMap, an online mapping product developed by the U.S. Geological Survey (USGS) that displays the distribution of ground shaking following an earthquake. ShakeMap ground-motion estimates are considered the best estimates of regional ground shaking because they are based on strong-motion recordings and, in areas having no recordings, empirical ground-motion prediction equations. ShakeMap products are developed for peak ground acceleration (PGA), peak ground velocity (PGV), and spectral acceleration at different

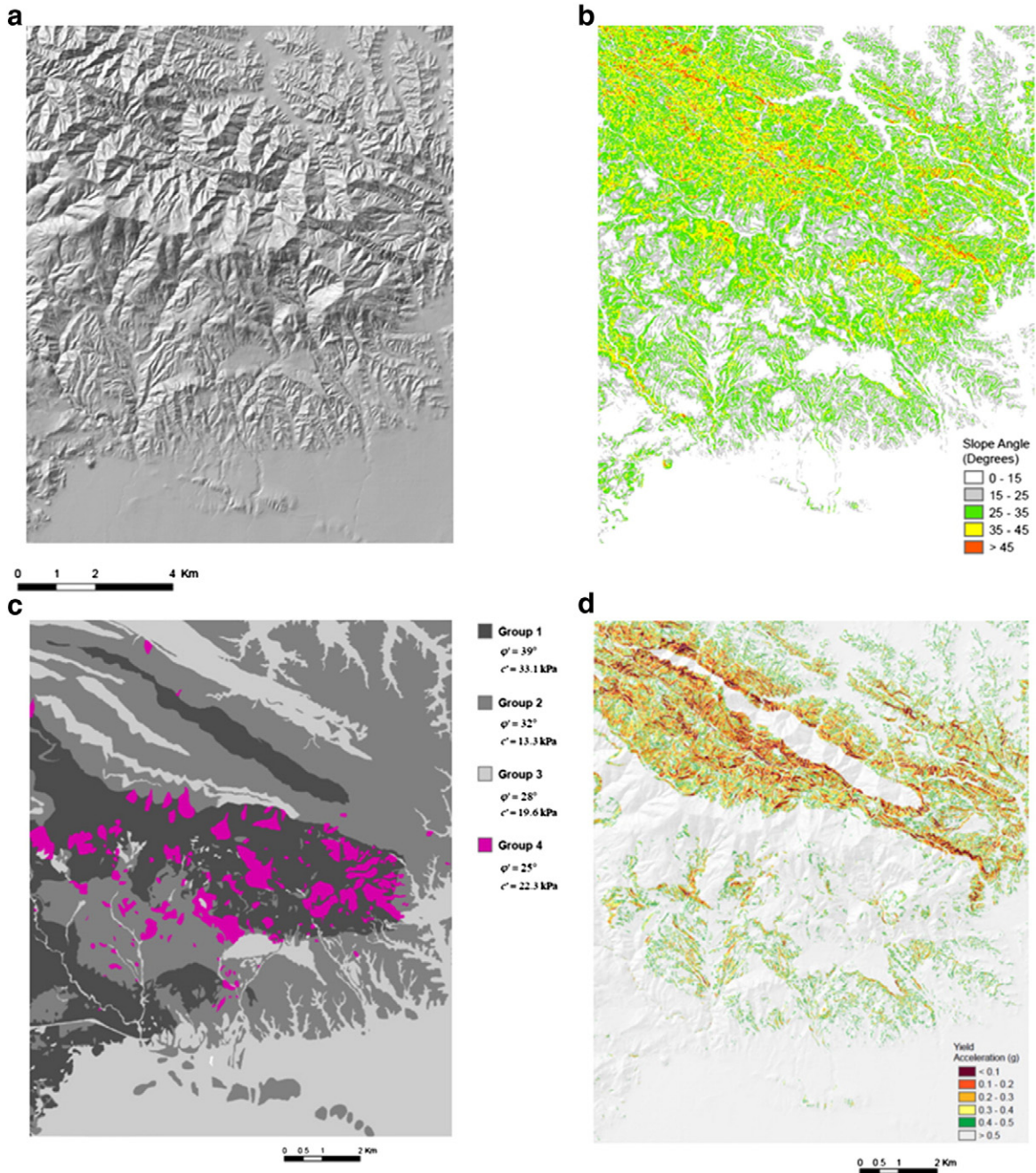


Fig. 4. Maps showing (a) shaded relief, (b) slope angle, (c) Strength Groups, and (d) k_y for the Oat Mountain quadrangle.

periods. For this study, the 1.5-km-gridded ShakeMap data for PGA and PGV for the Northridge earthquake were downloaded from the ShakeMap website (<http://earthquake.usgs.gov/earthquakes/shakemap/sc/shake/Northridge/>) and converted into 10-m raster grids using a simple kriging algorithm. Some sliding-displacement models characterize shaking in terms of the Arias intensity (I_a), but the ShakeMap website does not provide I_a data. To facilitate testing the displacement models that use I_a , we obtained gridded I_a values from the USGS (David Wald, personal communication) that were developed from the ShakeMap methodology and I_a values computed for each of the Northridge strong-motion recordings.

The resulting distributions of PGA , PGV , and I_a across the study area are shown in Fig. 6. As expected, the values of PGA , PGV , and I_a increase southeastward toward the earthquake fault rupture. Values of PGA range from about 0.2 g in the northwest corner of the Piru quadrangle to more than 0.8 g in the southern part of the Santa

Susana and Oat Mountain quadrangles. Values of PGV range from about 20 cm/s in the Piru quadrangle up to about 140 cm/s in the southeast corner of the Oat Mountain quadrangle. Values of I_a range from about 1 m/s in the Piru quadrangle to more than 10 m/s in some areas of the Oat Mountain quadrangle. The I_a values in Fig. 6 are significantly greater than those used by Jibson et al. (2000) but are considered better estimates of I_a for the Northridge earthquake because of the robust methodology used by ShakeMap.

3.3. Sliding displacement models

Empirical sliding-displacement prediction equations represent an efficient way to compute sliding-block displacements over a large area. Values of k_y and ground motion are combined within a GIS and median values of displacement are calculated for each cell in the study area. Each of the empirical models used in this study predicts sliding

Table 1
Shear strength properties assigned to geologic units.

Unit name (description)	Type	Piru		Val Verde		Newhall		Simi Valley		Santa Susana		Oat Mountain	
		ϕ' (°)	c' (kPa)	ϕ' (°)	c' (kPa)	ϕ' (°)	c' (kPa)						
Artificial fill	af	31	14.4	32	12.4	31	14.4	28	14.4			28	19.6
Artificial cut and fill	acf											28	19.6
Rockfall deposits	rf											28	19.6
Alluvium (young)	Qay											28	19.6
Pond deposits	Qp											28	19.6
Flood plain deposits	Qfp	31	14.4										
Alluvium	Qal	31	14.4	32	12.4	31	14.4	28	14.4	28	14.4	28	19.6
Older alluvium	Qao	25	34.7	32	12.4	31	14.4	28	14.4	28	14.4	28	19.6
Slope wash	Qsw					31	14.4			28	14.4	32	13.3
Caliche	Qc					31	14.4					28	19.6
Landslide deposits	Qls	12	14.1	13	15.6	25	12.0	23	22.5	23	22.5	25	22.3
Terrace deposits	Qt	31	14.4	32	12.4	31	14.4	28	14.4	28	14.4	28	19.6
Fan and terrace deposits	Qf/Qft	31	14.4	32	12.4					28	14.4		
Pacoima Fm. (ss/cg)	Qpa					31	14.4						
Older terrace deposits	Qto					31	14.4					28	19.6
Old fanglomerate	Qfo					31	14.4						
Saugus Fm.	Qs	31	14.4	32	12.4	31	14.4	35	12.0	35	12.0	32	13.3
Upper Member (silty breccia)	Qsu											32	13.3
Lower Member/Sunshine Ranch	Qsm							35	12.0	35	12.0	32	13.3
Saugus (Pelona Schist clasts)	Qsp			32	12.4	31	14.4						
Saugus (San Francisquito clasts)	Qss			32	12.4	31	14.4						
Pico Fm.	Tp	31	14.4	32	12.4			35	12.0	35	12.0	32	13.3
Pico Fm. (ss/cg)	Tpc	31	14.4	32	12.4	31	14.4			35	12.0	32	13.3
Pico Fm. (silt)	Tps	25	34.7	28	20.1	31	14.4			23	19.2	28	19.6
Towsley Fm. (ss/shale)	Tw									35	12.0	32	13.3
Towsley Fm. (shale)	Tws	31	14.4	28	20.1	37	14.8	23	19.2	28	19.6		
Towsley Fm. (ss)	Twc	31	14.4	32	12.4	37	14.8	35	12.0	32	13.3		
Hasley Conglomerate	Twhc	31	14.4	32	12.4								
Castaic Fm. (ss)	Tcs			28	20.1	37	14.8						
Mint Canyon Fm. (ss)	Tmc					37	14.8						
Mint Canyon Fm. (ss/clay)	Tmcl					37	14.8						
Modelo Fm. (shale)	Tm	31	14.4					35	12.0	35	12.0	39	31.3
Modelo Fm. (shale/mud)	Tm1	25	34.7					35	12.0	35	12.0	39	31.3
Modelo Fm. (porc. shale)	Tm2	31	14.4					35	12.0	35	12.0	39	31.3
Modelo Fm. (ss)	Tm3	31	14.4					35	12.0	35	12.0	39	31.3
Modelo Fm. (shale)	Tm4	31	14.4					35	12.0	35	12.0	39	31.3
Modelo Fm. (shale)	Tm5	31	14.4										
Modelo Fm. (diatom. shale)	Tmd									35	12.0	39	31.3
Modelo Fm. (shale)	Tms			28	20.1							39	31.3
Modelo Fm. (cg/ss)	Tmc			28	20.1								
Topanga Fm. (ss)	Tt							35	12.0	35	12.0	39	31.3
Topanga Fm. (basalt)	Ttb									28	14.4	39	31.3
Topanga Fm. (shale)	Tt1											39	31.3
Topanga Fm. (ss)	Tt2											39	31.3
Topanga Fm. (shale)	Tt3											39	31.3
Topanga Fm. (ss)	Tt4											39	31.3
Conejo Volcanics (andesite/basalt)	Tco							38	28.7				
Conejo Volcanics (andesite)	Tcoa							38	28.7				
Conejo Volcanics (basalt)	Tcob							38	28.7				
Rincon Shale	Trn	31	14.4										
Vaqueros Fm. (silt, ss)	Tv							35	12.0				
Sespe Fm. (ss, cg)	Ts	34	13.8					35	12.0	35	12.0		
Llajas Fm. (ss, silt, clay, cg)	Tl							35	12.0	35	12.0	39	31.3
Llajas Fm. (calc. ss, hard)	Tlc									35	12.0	39	31.3
Santa Susana Fm. (clay shale)	Tss									35	12.0	39	31.3
Simi Conglomerate	Tsc									35	12.0		
Simi Conglomerate (cg)	Tsc1											39	31.3
Simi Conglomerate (shale)	Tsc2											39	31.3
Simi Conglomerate (ss)	Tsc3											39	31.3
Chatsworth Fm. (ss)	Kc									38	28.7	39	31.3

ϕ' : effective angle of internal friction; c' : effective cohesion intercept; ss: sandstone; cg: conglomerate; 1 kPa = 20.885 lb/ft².

displacement for rigid sliding masses. Rigid displacements are used for two reasons. First, most earthquake-induced landslides are fairly shallow falls and slides in brittle surficial rock and debris (Keefer, 1984) that are reasonably represented as rigid sliding blocks. Second, the rigid-sliding-block approach currently is the only practical model that can be applied on a regional scale. Seven displacement models, each of which uses different combinations of ground-motion parameters to characterize ground shaking, are used in this study. Three models are from Jibson (2007) and are labeled J-(I_a), J-(PGA), and J-(PGA, I_a) based

on the ground-motion parameters used in the model. Four models are from Saygili and Rathje (2008) and Rathje and Saygili (2009); they are labeled RS-(PGA, M), RS-(PGA, PGV), RS-(PGA, I_a), and RS-(PGA, PGV, I_a). Saygili and Rathje (2008) showed that including multiple ground motion parameters in a displacement model decreases the standard deviation in the prediction.

Fig. 7 compares the sliding displacements predicted by the seven empirical models for the ground shaking observed across the study area. Under the most intense shaking in the southeast corner of the

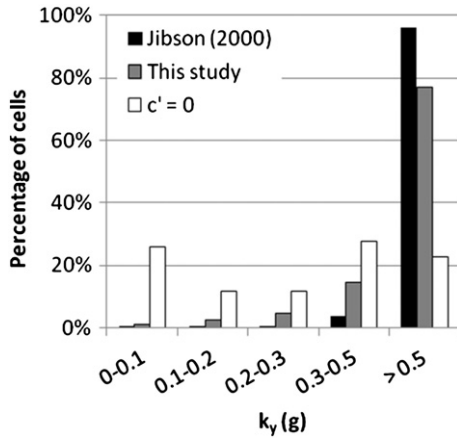


Fig. 5. Influence of assumed strength on distribution of k_y within the Oat Mountain quadrangle.

study area ($PGA \sim 0.65$ g, $PGV \sim 60$ cm/s, $I_a \sim 6$ m/s; Figure 7a), the RS models generally predict the largest displacements and the predictions fall within a relatively narrow range. The associated k_y thresholds that correspond to 5 cm of displacement range from 0.30 to 0.33 g. The J models predict smaller displacements that span a broader range, which results in a larger range of k_y thresholds (i.e., 0.17–0.26 g). Under less intense shaking in the northwest corner of the study area ($PGA \sim 0.3$ g, $PGV \sim 30$ cm/s, $I_a \sim 1.5$ m/s; Figure 7b), the RS models still tend to predict larger displacements than the J models, although the differences

are not as large as under the more intense shaking. Here, the k_y threshold corresponding to 5 cm of displacement ranges from 0.08 to 0.12 g across the seven models.

3.4. Evaluation metrics

An earthquake-induced landslide is considered likely if the predicted sliding displacement is greater than some threshold. Common displacement thresholds are 5 and 15 cm (California Geological Survey, 2004; Jibson and Michael, 2009), and predicted landslide locations are assessed based on these thresholds. The predicted landslide locations are compared to locations of landslides mapped by Harp and Jibson (1995, 1996). Mapped landslides include both the sources and deposits of the slides; only landslide source areas were considered in this analysis. Source areas were defined as those cells having elevations above the median elevation for each landslide; thus, the upper half of each landslide was considered a source area (Jibson et al., 2000). Landslide source areas comprise nearly 80,000 cells, or roughly 0.8% of the cells within the six-quadrangle study area.

In addition to measuring ground failures captured (%GFC), other metrics that are considered to evaluate the results are the percentage of the study area predicted to be landslides (%LS-pred) and the ratio between the predicted %LS and the observed %LS (%LS-pred/%LS-obs). These additional metrics are used to quantify false positive (incorrectly predicted landslide locations). Another metric that quantifies false positives is the false positive rate, which is defined as the percentage of the non-landslide cells predicted to be landslides. This metric was computed for each model tested but was found to be uninformative because the number of non-landslide cells was so much larger than the number of predicted landslide cells (i.e., about 99% of the study area did not

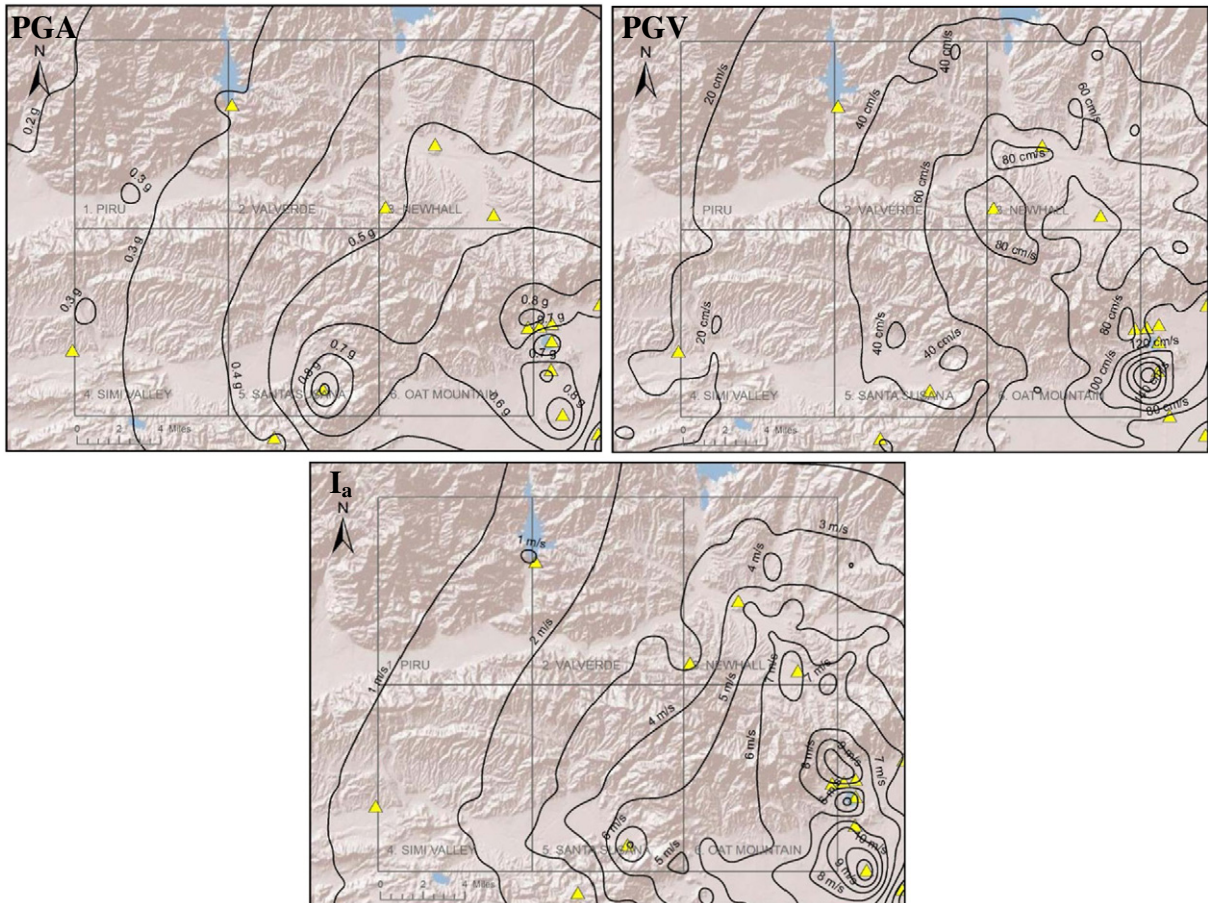


Fig. 6. Distribution of ground shaking across the study area during the Northridge earthquake.

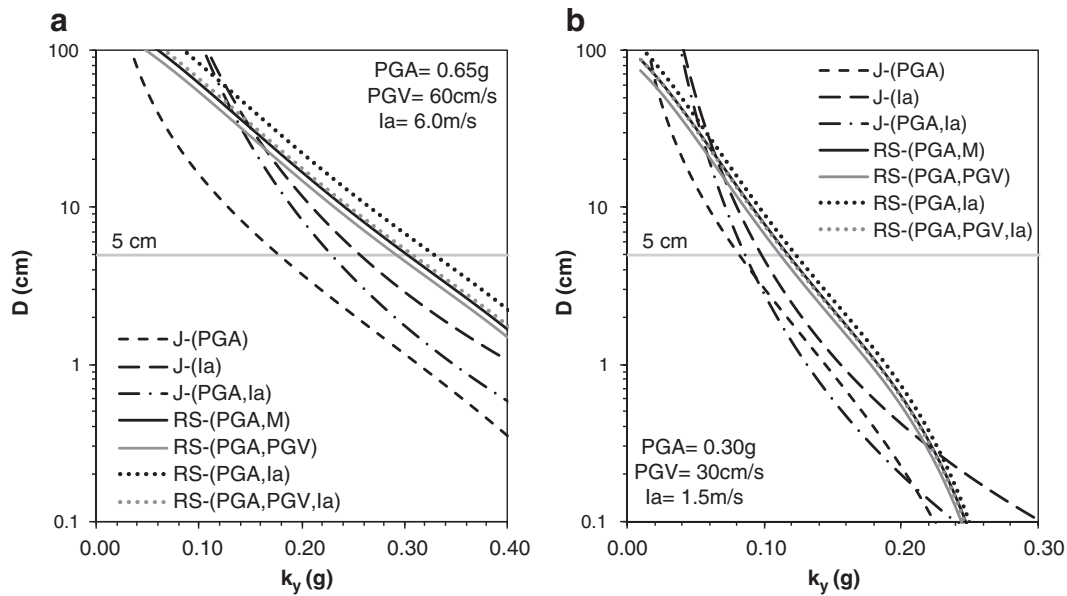


Fig. 7. Predicted displacements vs. k_y for the displacement models used in this study for ground shaking in (a) southeast section of study area and (b) northwest section of study area.

experience landslides) and all false positive rates were less than 10%. As a result, the metric %LS-pred/%LS-obs was considered a better measure of false positives.

4. Comparisons between landslide predictions and observations

4.1. Comparisons between different displacement models

Maps of predicted landslides for the Northridge earthquake were generated for each of the seven sliding displacement models and for displacement thresholds of 5 and 15 cm (Dreyfus, 2011). Fig. 8 shows the predicted landslides for a small area within the Oat Mountain quadrangle (see Figure 3 for location). This area contains geologic units from Strength Group 2 (Tw, Tpc, Qs with $c' = 13.3$ kPa, $\phi' = 32^\circ$) and Strength Group 3 (Tps, Qal/Qay with $c' = 19.6$ kPa, $\phi' = 28^\circ$). Fig. 8 shows predictions for the J-(I_a) and RS-(PGA, PGV) models and for displacement thresholds for 5 and 15 cm; mapped landslide source cells are overlain on the figure. The results show that in this area both the J-(I_a) and RS-(PGA, PGV) models do relatively well in capturing the general locations of observed landslides. The %GFC in this area is around 45–50% when using a displacement threshold of 15 cm, and it increases to 60–70% when using a displacement threshold of 5 cm. To achieve these accuracies the models are predicting approximately 4–6% of the area as landslides (%LS-pred) at a 15-cm threshold, and 10–15% of the area as landslides at a 5-cm threshold. The larger %LS-pred for the RS-(PGA, PGV) model is a direct result of the larger displacements predicted by this model for the ground-motion intensity observed in this area (Figure 7). The improved %GFC that occurs with a smaller displacement threshold comes at the expense of a larger %LS-pred. At the 15-cm threshold, the models predict landslide areas 1.5–2 times larger than observed (%LS-pred/%LS-obs = 1.5–2.0); at the 5-cm threshold the models predict 3–5 times larger landslide areas. Even though only about 50% of the landslides are captured and there is a large overestimation of the total landslide area, the predictions in Fig. 8 provide a qualitatively accurate depiction of where landslides were concentrated in this area during the Northridge earthquake.

Values of %GFC, %LS-pred, and %LS-pred/%LS-obs are computed across all six quadrangles using the seven empirical displacement models and displacement thresholds of 15 cm and 5 cm. The results are summarized in Fig. 9. At a threshold of 15 cm, the %GFC ranges from 19 to 29% for the seven models (Figure 9a), and it increases to 26–41% for a threshold of 5 cm. As noted previously, the improved

%GFC that occurs with the smaller displacement threshold is associated with a larger %LS-pred (Figure 9b) and larger %LS-pred/%LS-obs (Figure 9c). In some cases, the %LS-pred can be as much as 7–8 times larger than %LS-obs. The values reported in Fig. 9 represent the average over the six quadrangles, but results vary across the quadrangles (Dreyfus, 2011): the %GFC tends to be largest for the Oat Mountain quadrangle (as high as 55%) and smallest for the Newhall and Simi Valley quadrangles (as low as 10%).

The %GFC values do not differ appreciably among the displacement models. In fact, the %GFC values differ more among the quadrangles than among the models. The RS models generally capture 5–10% more of the landslides than the J models, but this comes at the expense of over-predicting the landslide area by a larger amount. Based on the data in Fig. 9 it is difficult to judge one model better than another because the results are so similar. However, the evaluation of the different displacement prediction models is overshadowed by the influence of the assigned shear strengths and their use across an entire geologic unit, as discussed in the next sections.

4.2. Influence of assigned shear strengths on predicted landslides

The influence of the assigned material shear strengths on the comparison between the predicted and observed landslides is evaluated using the RS-(PGA, PGV) model with a 5-cm displacement threshold. Three sets of shear-strength parameters are considered: the strengths used by Jibson et al. (2000), the strengths used in this study (Table 1), and the strengths used in this study with $c' = 0$ (the CGS approach). In general, the strengths from Jibson et al. (2000) are the highest and the strengths that use $c' = 0$ are the lowest. The influence of these different strengths on k_y is significant, as shown previously in Fig. 5.

Fig. 10 shows a comparison of observed and predicted landslides for the three sets of shear strengths. The rather high Jibson et al. (2000) strengths identify only a small number of landslides (Figure 10a). Across the Oat Mountain quadrangle, these strengths capture only about 7% of the landslide cells, and across all six quadrangles, only 3.3%. The %LS-pred/%LS-obs ratio for this case is only 0.14, which indicates a large under-prediction of the total landslide area. The lower strengths used in this study (Figure 10b) predict more landslides, with 55% of observed landslide cells captured in the Oat Mountain quadrangle and 41% across all six quadrangles. The %LS-pred/%LS-obs ratio for this case is 7.1, which indicates a large over-prediction of the landslide area. The CGS strength model with $c' = 0$ results in a very large number of predicted

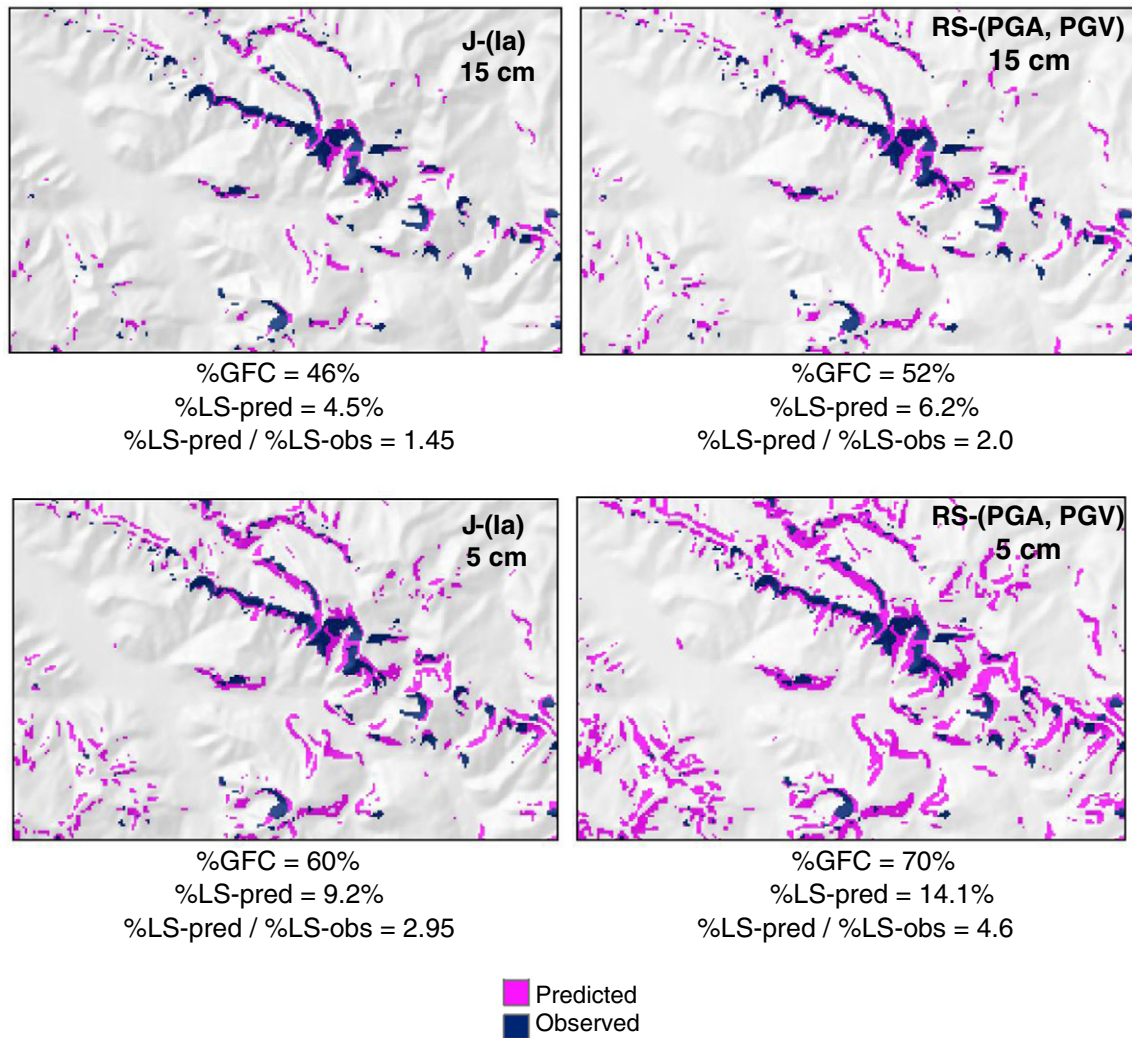


Fig. 8. Predicted and observed landslides based on different displacement models and displacement thresholds.

landslides (Figure 10c) and 95% of the observed landslide cells are captured across the six quadrangles. However, to achieve this large value of %GFC more than 40% of the study area is predicted as landslides (%LS-pred) and the %LS-pred/%LS-obs ratio is almost 50 (the predicted landslide area is 50 times larger than the observed landslide area).

These results show that increasing strengths across entire geologic units to ensure the static stability of steeper slopes within a geologic unit (i.e. the approach used by Jibson et al., 2000) results in predicted displacements that are too small to capture a large percentage of observed landslide cells. In contrast, ignoring any contribution of cohesion (i.e. the approach used by CGS) results in large predicted displacements across many flatter areas and grossly overestimates the area of earthquake-induced landslides.

4.3. Influence of assigning shear strengths based on geologic unit

To understand better how the geologic units and their assigned shear strengths influence the results of this study, the distribution of the observed, predicted, and accurately predicted landslides cells are listed in Table 2 as a function of geologic unit for the Oat Mountain quadrangle. Predictions in Table 2 are from the RS-(PGA, PGV) model with a 5-cm displacement threshold, which captured 55% of the landslide cells in this quadrangle.

The results in Table 2 show that no landslides are predicted within the geologic units included in Strength Group 1 (the strongest group) despite the fact that nearly 20% of the landslides observed in the Oat

Mountain quadrangle occurred within these geologic units. This observation points to a complication of using the strengths given in the CGS reports. Strength Group 1 includes the Modelo Formation (Table 1), a well-known landslide formation in southern California (Morton, 1971; Ziony et al., 1985; Parise and Jibson, 2000), but the assigned strengths are high ($c' = 31$ kPa, $\phi' = 39^\circ$, as compared to $c' = 26$ kPa, $\phi' = 31^\circ$ in Jibson et al., 2000). Strengths within the Modelo Formation vary considerably because of differences in lithology within the formation, which the CGS attempts to differentiate through identification of adverse (weaker) and favorable (stronger) bedding conditions. However, the geologic maps available for this study do not differentiate bedding conditions and the CGS report for the Oat Mountain quadrangle does not identify any adverse bedding locations within the quadrangle. Therefore, the Modelo Formation and all its sub-units are assigned to Strength Group 1, although strengths in many parts of the formation are likely lower.

The majority of observed landslides (~68%) occurred in Strength Group 2. If the Modelo Formation and its sub-units are included in Strength Group 2, about 80% of the landslides occurred in this strength group. The landslide predictions are relatively accurate within Strength Group 2; 74% of the observed landslide cells are correctly predicted across the entire strength group, and within the different geologic units 38–79% of the observed landslide cells are predicted correctly. However, the number of predicted landslide cells is much larger than observed (134,328 vs. 6,433; %LS-pred/%LS-obs = 21). The largest %GFC is 79% in the Towsley Formation (Tw), but the analysis predicts

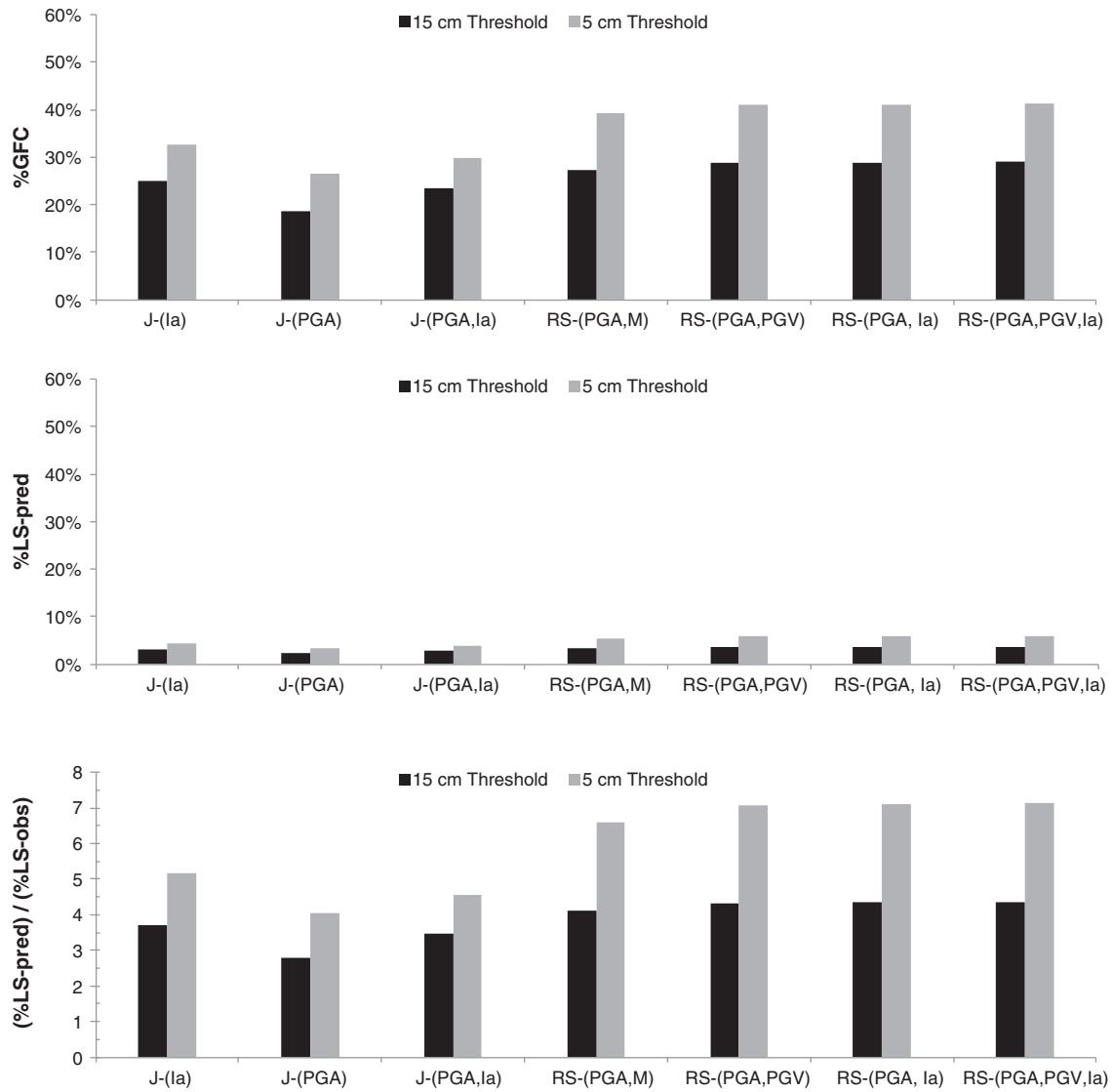


Fig. 9. Evaluation metrics compiled for the seven displacement models across the Northridge study area.

41% of that unit to be landslides, while only 1.6% of the unit actually experienced landslides.

Strength Group 3 accounts for about 13% of the observed landslides. Most of the geologic units in this strength group consist of Quaternary alluvial materials and artificial fills, both of which generally occur on very flat slopes. Almost all of the landslides in Strength Group 3 occur in units Tps and Tws, the only two units that crop out in steeper slopes. The %GFC is 30–50% for these geologic units.

Finally, Strength Group 4 represents mapped landslides and landslide deposits, and the strength assigned to these deposits is low to account for their presumably weakened nature. Only 1.1% of the observed landslides occur within these deposits, which is consistent with Keefer's (1984) observation from worldwide earthquakes that a relatively small proportion of seismically triggered landslides are reactivations of existing landslides. Despite the lower strength assigned to this group, only 7% of the observed landslide cells are captured. These observations from Strength Group 4 suggest that automatically assigning very low strengths to landslide deposits might be unwarranted.

4.4. Influence of slope angle

To investigate the relationship between landslides, geologic units/shear strengths, and slope angles, geologic units Tm (Modelo Formation

and sub-units Tm1/4/5/s in Strength Group 1), Tw (Towsley Formation in Strength Group 2), and Tps (Pico Formation in Strength Group 3) are considered. 55% of all landslide cells observed in the quadrangle are in these three units; 8.2% in the Tm units, 37.7% in the Tw unit, and 9.0% in the Tps unit (Table 2).

When a single shear strength is assigned to an entire geologic unit, the prediction of landslide displacement within that unit becomes predominantly a function of slope angle if it is assumed that the ground motions do not vary significantly across the geologic unit. Thus, a slope threshold can be computed that represents the slope angle above which landslides are predicted for the assigned shear strength in a geologic unit given a specific level of ground shaking. For example, using the average ground motions in the Oat Mountain quadrangle ($PGA = 0.65$ g, $PGV = 60$ cm/s, Figure 6) and the RS-(PGA, PGV) displacement model, a k_y of about 0.3 g will generate a displacement of 5 cm (Figure 7a). This k_y corresponds to slope angles of approximately 63°, 34°, and 39° for the shear strengths assigned to geologic units Tm, Tw, and Tps, respectively.

Fig. 11 shows for each of the three geologic units (1) the distribution of slope angles for all cells, (2) the distribution of slope angles for the observed landslide cells, and (3) the percentage of observed landslide cells within each slope-angle bin. The distribution of slope angles within the geologic units is similar for units Tm and Tps (~30–35% of slopes steeper than 30°), while the slopes in unit Tw are steeper (~55% of

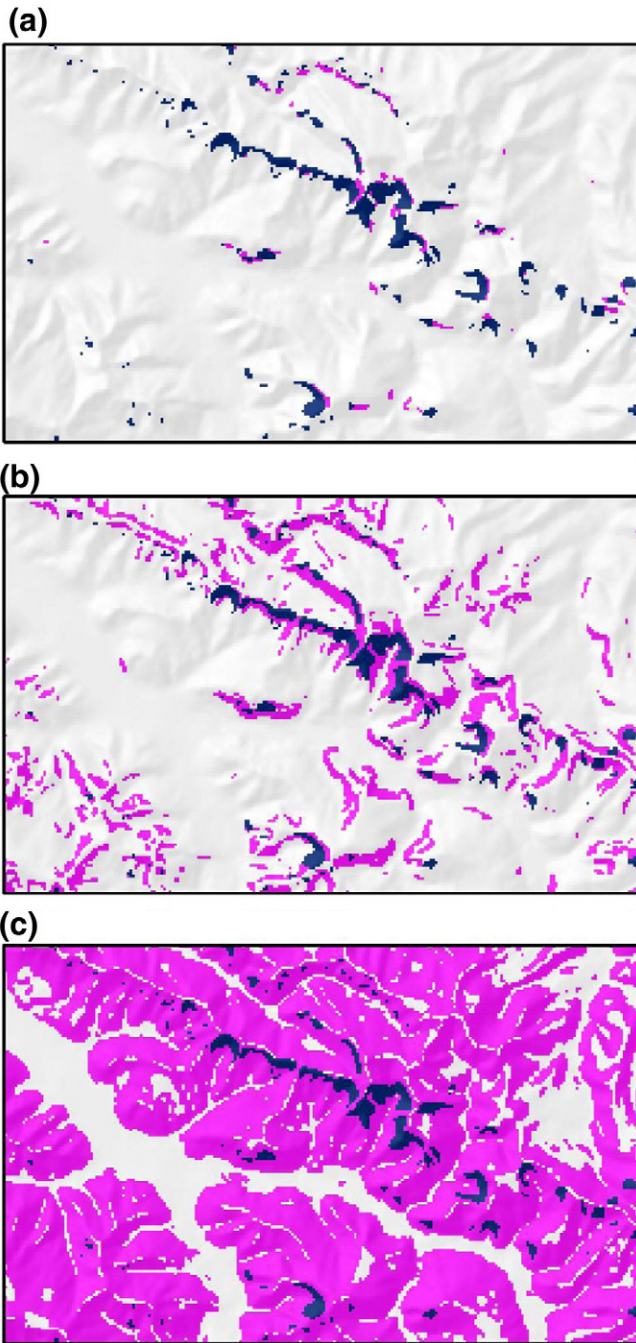


Fig. 10. Predicted locations of landslides using RS-(PGA, PGV) model, the 5 cm threshold, and strengths from (a) Jibson et al. (2000), (b) this study, and (c) ϕ' from this study with $c' = 0$.

slopes steeper than 30°). Slope-angle distributions for the landslide cells indicate that about 80% of the landslides occurred on slopes between 30° and 50° for all three geologic units, although a larger percentage occurred on steeper slopes for the Tw unit as compared with Tm and Tps. This result most likely is due to the larger number of steeper slopes in the Tw unit. Finally, the percentages of landslide cells within a slope-angle bin indicate that LS percentages increase as the slope angle increases. For the steepest slopes, the percentage of landslides can exceed 20% (e.g., $50\text{--}60^\circ$ for Tps). Although most landslides occur on $30^\circ\text{--}50^\circ$ slopes, the percentage of landslides within these slopes-angle bins is modest (1–10%) because these slope angles encompass much larger areas.

Fig. 11 also shows the slope thresholds for the three geologic units. As implemented in current mapping procedures, all slopes steeper than this specified threshold are predicted to fail. Therefore, the predicted

percentage of landslides within a slope-angle bin is 0% below the threshold and 100% above the threshold. No landslides are predicted, or captured, for the Tm unit because the large assigned shear strength results in the slope threshold being steeper than the steepest slopes in the unit. If Tm were assigned to Strength Group 2 (slope threshold 34°), 62% of the landslides would have been captured. For unit Tw, the %GFC is 79% (Table 2), which relates directly to the slope threshold of 34° and 79% of the landslides occurring on slopes steeper than 34° . Thus, all landslides on slopes steeper than 34° are captured. This comes, however, at the expense of predicting that 100% of these slopes will fail, although the observed landslide percentages within these slope-angle bins never approach 100% (Figure 11). Finally, the %GFC is smaller for unit Tps (%GFC = 32%, Table 2) because only 32% of the landslide occurred on slopes steeper than the slope threshold for this unit (39°).

The fact that the observed landslide percentages for a slope-angle bin within a given geologic unit never approach 100% (Figure 11) reveals important limitations with respect to the approaches currently used to predict earthquake-induced landslides on a regional scale. Although current approaches assign a single shear strength to a geologic unit, clearly spatial variability in that strength exists across the unit. This variability might explain why some steep slopes remain stable while some flat slopes fail within the same geologic unit, and it might also explain why some steeper slopes fail and others do not within the same geologic unit.

5. Discussion

The focus of this paper is not to argue that a rigid-sliding-block model is the best model for regional-scale evaluation of seismic landslide hazards. Rather, given this model's widespread usage, there is a need to determine which specific model types and inputs yield the best results. At regional scale, all models involve significant trade-offs between utility and accuracy because it is not practical to conduct a detailed stability analysis of every slope. Instead, the objective is to use the best available regional-scale data in the best available model to produce the best possible estimate of slope behavior. By comparing results of different model types and input data with a database of thousands of landslides, a statistical picture is obtained of the relative effectiveness of different model types and inputs.

Significant research has taken place over the last decade regarding the identification of the ground-motion parameters that best predict the earthquake response for a variety of systems (e.g., Kramer and Mitchell, 2006 for liquefaction response, Travasarou and Bray, 2003; Saygili and Rathje, 2008 for slope displacements). These previous studies used results from numerical simulations to identify the most useful ground-motion parameters. This study uses field observations to evaluate models that use different ground-motion parameters. Using field data always introduces more uncertainty than using numerical simulations, but the field data provide a realistic assessment of whether improvements indicated by numerical simulation are warranted. The results from this study indicate that the various displacement models produce similar results, and therefore further enhancements to displacement-prediction models will not improve regional seismic landslide predictions.

The results of this study also indicate that the approach used to assign shear strengths is critical. Although this finding might not be surprising, this study quantifies the significance of the effect. Nonetheless, comparing model results using different sources of shear strengths must be done with an understanding of the original rationales for those strengths. The CGS strengths with $c' = 0$ originally were selected not to accurately predict landslide locations but to produce zoning maps that would be used to trigger a regulatory process for certain land uses. For this reason, CGS uses very conservative strengths by ignoring cohesion so as to capture every area that might conceivably have landslide problems rather than to optimize the trade-off between %GFC, %LS-pred, and %LS-obs. The Jibson et al. (2000) strengths originally were selected to capture differences in strengths between units in a model whose purpose was to determine if larger predicted sliding displacement related to an

Table 2
Distribution of observed and predicted landslide cells across geologic units in the Oat Mountain quadrangle using Model RS-(PGA, PGV) and a 5 cm threshold.

Strength group	ϕ (°)	c'(kPa)	Geologic Unit	Observed LS cells			Predicted LS cells		Accurate	
				Cells	% of LS cells	% of G. unit	Cells	% of G. unit	Cells	%GFC in G. unit
1	39	31.3	Tl	49	0.52%	1.9%	0	0.0%	0	0.0%
1	39	31.3	Tlc	0	0.0%	0.00%	0	0.0%	0	0.0%
1	39	31.3	Tss	6	0.06%	0.56%	0	0.0%	0	0.0%
1	39	31.3	Tsc1	5	0.05%	0.08%	0	0.0%	0	0.0%
1	39	31.3	Tsc2	2	0.02%	0.04%	0	0.0%	0	0.0%
1	39	31.3	Tsc3	126	1.3%	1.4%	0	0.0%	0	0.0%
1	39	31.3	Kc	166	1.8%	0.22%	0	0.0%	0	0.0%
1	39	31.3	Tm	395	4.2%	0.52%	0	0.0%	0	0.0%
1	39	31.3	Tm1/4/5/s	373	4.0%	0.38%	0	0.0%	0	0.0%
1	39	31.3	Tm2	66	0.7%	0.36%	0	0.0%	0	0.0%
1	39	31.3	Tm3	14	0.15%	0.15%	0	0.0%	0	0.0%
1	39	31.3	Tmd	252	2.7%	3.3%	0	0.0%	0	0.0%
1	39	31.3	Tt	128	1.4%	0.81%	0	0.0%	0	0.0%
1	39	31.3	Ttb	21	0.22%	1.4%	0	0.0%	0	0.0%
1	39	31.3	Tt1/3	6	0.06%	0.40%	0	0.0%	0	0.0%
1	39	31.3	Tt2/4	79	0.84%	0.74%	0	0.0%	0	0.0%
Total (Strength Group 1)				1688	17.9%		0		0	0.0%
2	32	13.3	Tp	145	1.54%	1.0%	1461	10.2%	74	51.0%
2	32	13.3	Tpc	1275	13.5%	2.5%	13,004	25.5%	928	72.8%
2	32	13.3	Qsw	16	0.17%	0.03%	908	1.7%	10	62.5%
2	32	13.3	Tw	3559	37.7%	1.7%	87,541	40.8%	2810	79.0%
2	32	13.3	Twc	557	5.9%	1.1%	18,304	36.7%	419	75.2%
2	32	13.3	Qs	402	4.3%	0.27%	6016	4.1%	268	66.7%
2	32	13.3	Qsu	50	0.53%	0.10%	2626	5.0%	19	38.0%
2	32	13.3	Qsm	429	4.5%	0.47%	4468	4.9%	204	47.6%
Total (Strength Group 2)				6433	68.1%		134,328		4732	73.6%
3	28	19.6	acf, af	16	0.17%	0.32%	42	0.84%	10	62.5%
3	28	19.6	rf	0	0.0%	0.0%	0	0.0%	0	0.0%
3	28	19.6	Qc	0	0.0%	0.0%	9	0.4%	0	0.0%
3	28	19.6	Tps	845	9.0%	1.5%	2806	5.0%	272	32.2%
3	28	19.6	Tws	349	3.7%	1.1%	4498	13.8%	174	49.9%
3	28	19.6	Qal, Qay/1/2, Qp	1	0.01%	0.00%	127	0.04%	0	0.0%
3	28	19.6	Qao	9	0.10%	0.02%	81	0.20%	1	11.1%
3	28	19.6	Qt	0	0.0%	0.0%	10	0.41%	0	0.0%
3	28	19.6	Qto	1	0.01%	0.05%	11	0.53%	1	100.0%
Total (Strength Group 3)				1221	12.9%		7584		458	37.5%
4	25	22.3	Qls	103	1.1%	0.14%	1506	2.1%	7	6.8%
Total (Strength Group 4)				103	1.1%		1506		7	6.8%

increased likelihood of failure. Jibson et al. (2000) did not use threshold displacements to predict failure in a binary fashion as was done in this study; they simply quantified the relationship between predicted sliding displacement and probability of failure. The strengths used in this paper are best suited to the objectives of this study: to evaluate the utility of existing procedures for mapping seismic landslide hazards by comparing threshold values of sliding displacement with actual landslide distributions.

Based on the results of this study, the one key issue that requires further study is the quantification of intra-formational variation in shear strength. Mapping differences in shear strength within geologic units is daunting because geology is mapped on the basis of lithology, depositional environment, and age, not on the basis of geotechnical properties. Geologic formations commonly contain interbedded sequences of rock

having profoundly different physical characteristics (e.g., interbedded sandstone and siltstone). The Modelo Formation discussed in this paper is an excellent example of this issue. One approach to solve this problem is to map strength differences in the field, but this approach is extremely time-consuming and requires collecting and testing a significant number of material samples. Another possibility is to use remote sensing via multi-spectral or hyperspectral sensors to map strength differences, but significant research is required to achieve this goal. While a solution to this problem currently does not exist, this study demonstrates that it is perhaps the most critical issue towards developing more accurate regional predictions of seismic landslides.

Finally, an additional factor that limits the ability of current models to capture a high percentage of triggered landslides is local variability of ground shaking due to topographic amplification. Several studies of

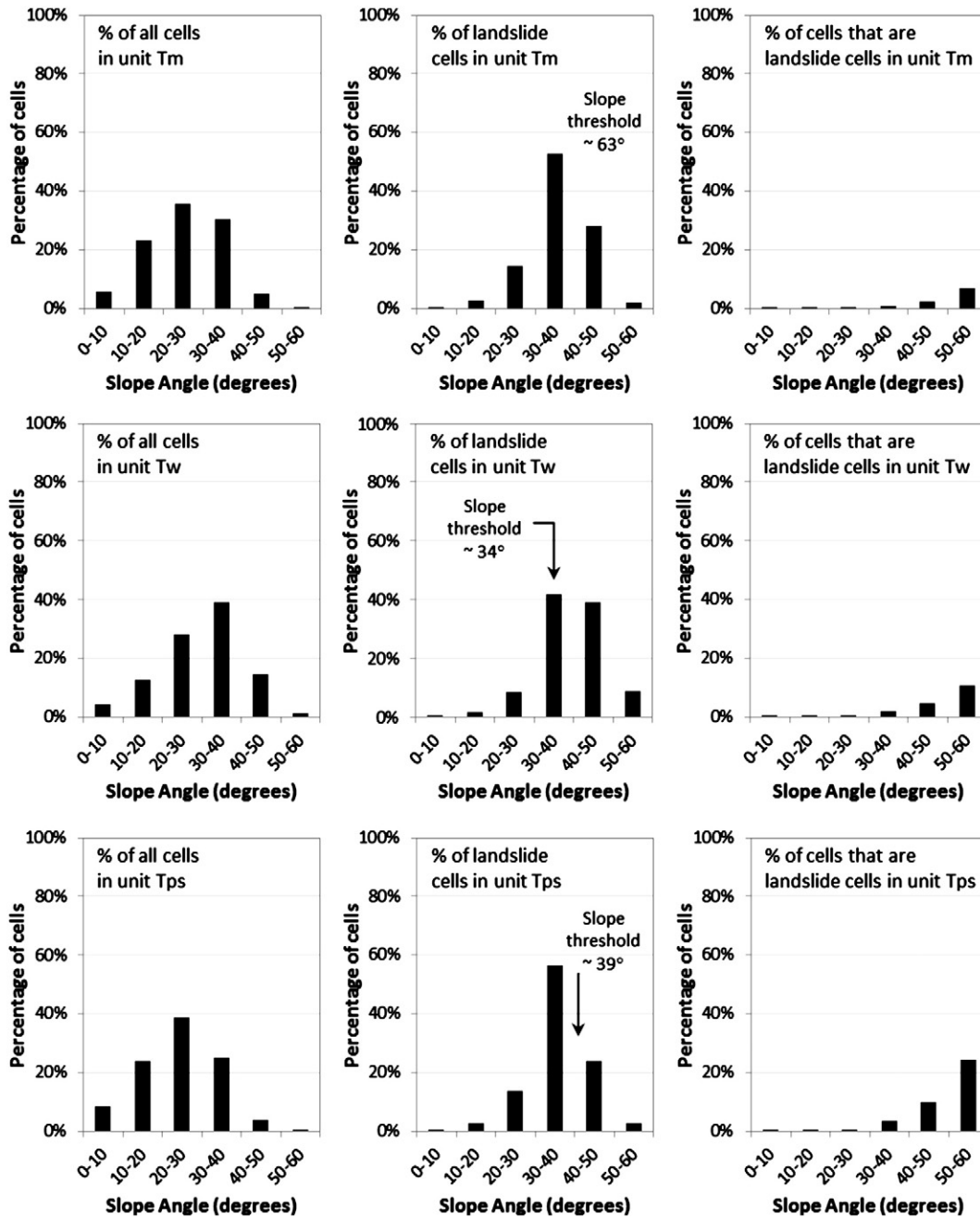


Fig. 11. Distribution of slope angles for all cells, distribution of slope angles for observed landslide cells, and percentage of observed landslide cells within each slope angle bin for the Oat Mountain quadrangle within geologic units Tm (Strength Group 1), Tw (Strength Group 2), and Tps (Strength Group 3).

the Northridge earthquake documented the role of topographic amplification on the triggering of landslides (Harp and Jibson, 1995, 1996, 2002; Sepúlveda et al., 2005; Meunier et al., 2008). The regional estimates of ground shaking from ShakeMap account for local ground-motion recordings, but they potentially ignore important localized topographic effects, particularly near the crests of ridges. Although a detailed treatment of the effects of topographic amplification is beyond the scope of this paper, it is well documented both theoretically and observationally, and it likely contributes to the limited ability of current models to predict a large percentage of landslide locations.

6. Summary and conclusions

To have confidence in regional seismic landslide hazard maps the methodologies used to derive these maps need to be compared with

and validated against field observations of landslide occurrence during previous, well-documented earthquakes. The 1994 Northridge earthquake represents one of the most well-documented earthquakes in terms of earthquake-induced landslides, and this paper uses the observed landslides from that earthquake to evaluate the methodologies used to predict earthquake-induced landslides on a regional scale. This study improves on previous comparisons with the Northridge earthquake landslide dataset by using the latest empirical prediction models for sliding displacement, many of which incorporate multiple ground-motion parameters, and by using ground-shaking estimates from ShakeMap, which is the state-of-the-art in the regional characterization of earthquake ground shaking.

The distribution of k_y across the study area significantly affects the predicted displacements, and this distribution is influenced predominantly by the assigned shear strengths. Increasing the shear strength

across an entire geologic unit to ensure the static stability of the steeper slopes within the unit artificially increases the k_y values for flatter slopes within that unit and underestimates the seismic landslide hazard. Ignoring the contribution of cohesion to the shear strength generates significantly smaller values of k_y and overestimates the seismic landslide hazard. We recommend using best estimate values of c' and ϕ' , applied with engineering judgment and associated with an appropriate sliding-block thickness, because this approach provides the most likely distribution of k_y values across a region.

Seven empirical displacement models were used in this study. These models predict sliding block displacement as a function of k_y and various combinations of the ground motion parameters PGA , PGV , and I_a . The ability of each of these models to predict the landslide distribution from the Northridge earthquake was quantified. Each of these models was used along with displacement thresholds of 5 and 15 cm to predict the occurrence of landslides based on the k_y and ground-motion distributions. At a threshold of 15 cm, the seven models captured 19–29% of the observed landslides; at a threshold of 5 cm the models captured 26–41% of the observed landslides. These ground-failure capture percentages are associated with a general over-prediction of total landslide area by a factor of 4–7. The ground-failure-capture percentages do not differ appreciably among the different displacement models; this suggests that the choice of model is less important than other factors such as the assignment of shear strengths and the characterization of ground motion.

Using of a single shear strength for an entire geologic unit results in all slopes steeper than a threshold slope angle being predicted to fail during the earthquake. Observed landslide percentages for a slope-angle bin within a geologic unit never approach 100%, which indicates that spatial variations in shear-strength properties exist and affect the observed landslide distributions. To improve regional seismic landslide hazard maps, we recommend that robust methods to incorporate the spatial variability in shear strength be developed. Improvements to displacement-prediction models for regional applications are not required until the strength issue is resolved.

Acknowledgments

Financial support for this work was provided by the U.S. Geological Survey (USGS), Department of the Interior, under grant G09AP00131. This support is gratefully acknowledged. The views and conclusions contained in this document are those of the authors and should not be interpreted as necessarily representing the official policies, either expressed or implied, of the U.S. Government.

References

Arias, A., 1970. A measure of earthquake intensity. In: Hansen, R.J. (Ed.), *Seismic Design for Nuclear Power Plants*. Massachusetts Institute of Technology Press, Cambridge, MA, pp. 438–483.

California Department of Conservation, 1997a. Seismic hazard zone report for the Newhall 7.5-Minute quadrangle, Los Angeles County, California. California Division of Mines and Geology Seismic Hazard Zone Report 04 (60 pp.).

California Department of Conservation, 1997b. Seismic hazard zone report for the Oat Mountain 7.5-Minute quadrangle, Los Angeles County, California. California Division of Mines and Geology Seismic Hazard Zone Report 05 (58 pp.).

California Department of Conservation, 1997c. Seismic hazard zone report for the Simi Valley East and Simi Valley West 7.5-Minute quadrangles, Ventura and Los Angeles Counties, California. California Division of Mines and Geology Seismic Hazard Zone Report 002 (59 pp.).

California Department of Conservation, 2002a. Seismic hazard zone report for the Piru 7.5-Minute quadrangle, Ventura County, California. California Division of Mines and Geology Seismic Hazard Zone Report 074 (54 pp.).

California Department of Conservation, 2002b. Seismic hazard zone report for the Val Verde 7.5-Minute quadrangle, Los Angeles and Ventura Counties, California. California Division of Mines and Geology Seismic Hazard Zone Report 076 (52 pp.).

California Geological Survey, 2004. Recommended criteria for delineating seismic hazard zones in California: California Geological Survey Special Publication, 118 (12 pp.).

California Geological Survey, 2013. Seismic Hazards Zonation Program. <http://www.conservacion.ca.gov/cgs/shzp/Pages/Index.aspx> (Accessed January 10, 2013).

Carro, M., De Amicis, M., Luzi, L., Marzorati, S., 2003. The application of predictive modeling techniques to landslides induced by earthquakes: the case study of the 26 September 1997 Umbria-Marche earthquake (Italy). *Engineering Geology* 69, 139–159.

Dreyfus, D.K., 2011. A Comparison of Methodologies Used to Predict Earthquake-Induced Landslides. (M.S. thesis) University of Texas at Austin (149 pp.).

Godt, J.W., Şener, B., Verdin, K.L., Wald, D.J., Earle, P.S., Harp, E.L., Jibson, R.W., 2009. Rapid assessment of earthquake-induced landsliding. *Proceedings of the First World Landslides Forum*, Tokyo, Japan, pp. 219–222.

Harp, E.L., Jibson, R.W., 1995. Inventory of landslides triggered by the Northridge, California earthquake. U.S. Geological Survey Open-File Report 95-213 (17 pp.).

Harp, E.L., Jibson, R.W., 1996. Landslides triggered by the 1994 Northridge, California earthquake. *Bulletin of the Seismological Society of America* 86, S319–S332.

Harp, E.L., Jibson, R.W., 2002. Anomalous concentrations of seismically triggered rock falls in Pacoima Canyon: are they caused by highly susceptible slopes or local amplification of seismic shaking? *Bulletin of the Seismological Society of America* 92, 3180–3189.

Jibson, R.W., 2007. Regression models for estimating coseismic landslide displacement. *Engineering Geology* 91, 209–218.

Jibson, R.W., Michael, J.A., 2009. Maps showing seismic landslide hazards in Anchorage, Alaska. U.S. Geological Survey Scientific Investigations Map 3077 (11 pp.).

Jibson, R.W., Harp, E.L., Michael, J.A., 2000. A method for producing digital probabilistic seismic landslide hazard maps. *Engineering Geology* 58, 271–289.

Keefer, D.K., 1984. Landslides caused by earthquakes. *Geological Society of America Bulletin* 95, 406–421.

Kramer, S.L., Mitchell, R.A., 2006. Ground motion intensity measures for liquefaction hazard evaluation. *Earthquake Spectra* 22 (2), 413–438.

McCrink, T.P., 2001. Regional earthquake-induced landslide mapping using Newmark displacement criteria, Santa Cruz County, California. In: Ferriz, H., Anderson, R. (Eds.), *Engineering Geology Practice in Northern California: California Division of Mines and Geology Bulletin 210/Association of Engineering Geologists Special Publication*, 12, pp. 77–92.

Meunier, P., Hovius, N., Haines, J.A., 2008. Topographic site effects and the location of earthquake induced landslides. *Earth and Planetary Science Letters* 275, 221–232.

Morton, D.M., 1971. Seismically triggered landslides in the area above the San Fernando Valley. The San Fernando Valley, California, earthquake of February 9, 1971: U.S. Geological Survey Professional Paper, 733, pp. 99–104.

Newmark, N., 1965. Effects of earthquakes on dams and embankments. *Geotechnique* 15, 139–160.

Parise, M., Jibson, R.W., 2000. A seismic landslide susceptibility rating of geologic units based on analysis of characteristics of landslides triggered by the January 17, 1994, Northridge, California, earthquake. *Engineering Geology* 58, 251–270.

Rathje, E.M., Saygili, G., 2009. Probabilistic assessment of earthquake-induced sliding displacements of natural slopes. *Bulletin of the New Zealand Society for Earthquake Engineering* 42, 18–27.

Saygili, G., Rathje, E.M., 2008. Empirical predictive models for earthquake-induced sliding displacements of slopes. *Journal of Geotechnical and Geoenvironmental Engineering* 134, 790–803.

Sepúlveda, S.A., Murphy, W., Jibson, R.W., Petley, D.N., 2005. Seismically induced rock slope failures resulting from topographic amplification of strong ground motions: the case of Pacoima Canyon, California. *Engineering Geology* 80, 336–348.

Travasariou, T., Bray, J.D., 2003. Optimal ground motion intensity measures for assessment of seismic slope displacements, 2003 Pacific Conference on Earthquake Engineering, Christchurch, New Zealand.

U.S. Geological Survey, 2012. ShakeMaps. <http://earthquake.usgs.gov/earthquakes/shakemap/> (Accessed December 15, 2012).

Wilson, R.C., Keefer, D.K., 1983. Dynamic analysis of a slope failure from the 6 August 1979 Coyote Lake, California earthquake. *Bulletin of the Seismological Society of America* 73, 863–877.

Yerkes, R.F., Campbell, R.H., 1995a. Preliminary geologic map of the Newhall 7.5-minute quadrangle, southern California: a digital database. U.S. Geological Survey Open-File Report 95-800.

Yerkes, R.F., Campbell, R.H., 1995b. Preliminary geologic map of the Oat Mountain 7.5-minute quadrangle, southern California: a digital database. U.S. Geological Survey Open-File Report 95-89.

Yerkes, R.F., Campbell, R.H., 1995c. Preliminary geologic map of the Piru 7.5-minute quadrangle, southern California: a digital database. U.S. Geological Survey Open-File Report 95-801.

Yerkes, R.F., Campbell, R.H., 1995d. Preliminary geologic map of the Val Verde 7.5-minute quadrangle, southern California: a digital database. U.S. Geological Survey Open-File Report 95-699.

Yerkes, R.F., Campbell, R.H., 1997a. Preliminary geologic map of the Santa Susana 7.5-minute quadrangle, southern California: a digital database. U.S. Geological Survey Open-File Report 97-258.

Yerkes, R.F., Campbell, R.H., 1997b. Preliminary geologic map of the Simi 7.5-minute quadrangle, southern California: a digital database. U.S. Geological Survey Open-File Report 97-259.

Ziony, J.I., Evernden, J.F., Fumal, T.E., Harp, E.L., Hartzell, S.H., Joyner, W.B., Keefer, D.K., Spudich, P.A., Tinsley, J.C., Yerkes, R.F., Youd, T.L., 1985. Predicted geologic and seismologic effects of a postulated magnitude 6.5 earthquake along the northern part of the Newport-Inglewood fault zone. In: Ziony, J.I. (Ed.), *Evaluating Earthquake Hazards in the Los Angeles Region—An Earth-Science Perspective*: U.S. Geological Survey Professional Paper, 1360, pp. 415–442.